Front. Phys., 2012, 7(4): 424–428
DOI 10.1007/s11467-011-0241-9

RESEARCH ARTICLE

Electric field driven phase transition and possible twining quasi-tetragonal phase in compressively strained $BiFeO_3$ thin films

Cheng-Liang Lu (陆成亮)[1,*], **Jun-Ming Liu** (刘俊明)[2,3,†], **Tao Wu** (吴韬)[4]

[1] *School of Physics, Huazhong University of Science and Technology, Wuhan 430074, China*
[2] *Laboratory of Solid State Microstructure, Nanjing University, Nanjing 210093, China*
[3] *International Center for Materials Physics, Chinese Academy of Sciences, Shenyang 110016, China*
[4] *Division of Physics and Applied Physics, School of Physical and Mathematical Sciences, Nanyang Technological University, Singapore 637371, Singapore*

*E-mail: * cllu@mail.hust.edu.cn, † liujm@nju.edu.cn*
Received November 6, 2011; accepted November 29; 2011

Highly compressively strained $BiFeO_3$ thin films with different thickness are epitaxially grown on (001) $LaAlO_3$ substrates and characterized using various techniques. The quasi-tetragonal phase with a giant axial ratio of ~ 1.25 and its thickness-dependent evolution are investigated. An interesting twining structure of the quasi-tetragonal phase is evidenced in thicker films through detailed reciprocal space mapping, which becomes more pronounced with increasing film thickness. Moreover, an interesting electric-field driven phase transition was evidenced in the film with a thickness of 38 nm, in which the quasi-tetragonal and rhombohedral phases are close to each other in energy landscape.

Keywords ferroelectricity, antiferromagnetic, phase transition

PACS numbers 77.80.-e, 75.50.Ee, 77.80.Bh

Multiferroic materials have been intensively studied because of the simultaneous coexistence of multi-polar parameters with intimate cross-coupling, which brings out novel physical phenomena and offers possibilities for unprecedented functionalities [1–4]. $BiFeO_3$ (BFO) is arguably the most studied multiferroic material due to its unique above room temperature ferroelectricity (Curie temperature $T_C \sim 1103$ K) and antiferromagnetism (Nèel temperature $T_N \sim 643$ K) [5]. Very recently, some fascinating physical properties, such as over-bandgap photovoltaic effect [6] and enhanced piezoelectricity after doping [7–9], were discovered, which makes BFO a focus of intensive attention in multiferroic research.

At room temperature bulk BFO has a rhombohedral (R) structure (space group $R3c$) with cell parameters of $a = 3.96$ Å and $a_r \sim 89.4°$ [10]. The spontaneous polarization (P) along the pseudocubic $\langle 111 \rangle$ directions originates from the bismuth lone pairs [11] and is as high as 100 μC/cm^2. Recently, first-principles calculations predicted that a metastable tetragonal (T) phase with a giant axial ratio (~ 1.27) and an extremely large spontaneous polarization of $P \sim 150$ μC/cm^2 can be achieved in BFO under a compressive strain [12]. Indeed, the giant axial ratio ($c/a \sim 1.27$) and large spontaneous polarization ($P \sim 150$ μC/cm^2 for pure T-phase BFO) were confirmed by several recent experiments on BFO thin films grown on (001) $LaAlO_3$ (LAO) [13–16]. The mechanism of the large P in T-phase BFO was ascribed to the displacement of Fe^{3+} relative to the oxygen octahedral, which indicates that the magnetic cation Fe^{3+} can simultaneously contribute to ferroelectricity and magnetism [16]. Besides the giant axial ratio and extremely large spontaneous polarization in T-phase BFO, people have revealed quite complex crystalline structure of the highly strained BFO [17, 18], in which there remain open questions regarding this T-phase BFO. Zeches *et al.* observed an exotic morphotropic phase boundary (MPB) like phenomenon in BFO/LAO, in which R-phase and T-phase coexisted with each other and a smooth transition between the phases was identified [14]. However, a very

© Higher Education Press and Springer-Verlag Berlin Heidelberg 2012

sharp structure phase transition caused by the compressive strain was predicted by first-principles calculations [19, 20]. Moreover, an in-plane (IP) nano-scale stripe domain of the quasi-T phase BFO was revealed by Chen *et al.* [21], while it was not detected in previous works on BFO/LAO thin films [13, 14]. These phenomena strongly suggest an unanticipated and rather complex structure of the highly compressively strained BFO thin film, and detailed structure investigations are necessary in getting a better understanding on this topic.

In this work, high quality BFO thin films were deposited on LAO substrates with a large misfit strain of $\sim 4.8\%$, which were carefully examined using high resolution X-ray diffraction (HRXRD) and piezoresponse force microscopy (PFM). Our results revealed clear stripe domains and twining structures of the quasi-T phase BFO. Furthermore, interesting electric field driven structure phase transition was evidenced for such highly strained BFO/LAO thin films.

BFO thin films with different thickness ($19 \leqslant t \leqslant 114$ nm) were grown on (001) $LaAlO_3$ substrates using pulsed laser deposition (PLD) at 700 ℃ in 100 mTorr oxygen. A KrF excimer laser ($\lambda = 248$ nm) was used with an energy density of ~ 1.3 J/cm^2 and a repetition rate of 5 Hz, as reported previously [22]. The topographic imaging and PFM measurements were carried out on an atomic force microscope (AFM) (Asylum Research MFP-3D). By conducting AFM tips (Pt/Ir-coated Si) we measured the local piezoresponse and topography simultaneously [23]. Detailed crystalline structure investigations, including the normal θ–2θ scans and the symmetric/asymmetric reciprocal space mappings (RSM), were carried out using a HRXRD of Rigaku.

Figure 1 presents X-ray $\theta-2\theta$ scans of BFO/LAO thin films with different thickness. No impurity phase was detected. The out-of-plane lattice parameter of BFO films calculated from the (00l) peaks is ~ 4.66 Å, which is much larger than that of the R-phase due to the compressive strain ($\sim 4.8\%$) [4]. This is in agreement with the previous reports on BFO/LAO thin films [13, 14]. Increasing the film thickness led to strain relaxation as well as another diffraction peak (indicated by solid triangles) corresponding to $c \sim 4.13$ Å, which can be assigned to the R-phase [14]. The strain relaxation also causes a systematic increase in c of the quasi-T phase, which was evidenced by the shift of the (002) peaks towards smaller angles. In addition, the presence of multiple internal interference peaks in the sample with $t = 38$ nm (indicated by open triangle) confirms the uniformity and epitaxy of the film.

The topography and the out-of-plane/in-plane (OOP/IP) PFM images are presented in Figs. 2(a)–(c). Uniform OOP piezoelectric response was observed, indicating that the polarization vectors largely point downwards. In contrast, the surface morphology and the

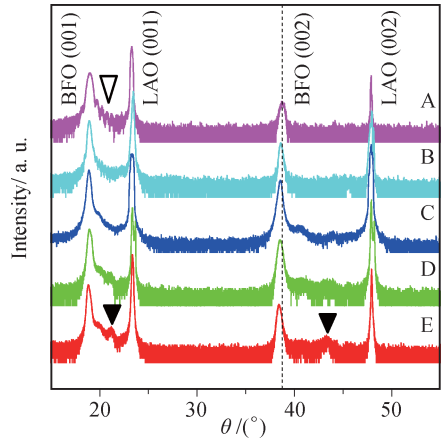

Fig. 1 X-ray diffraction spectra of BFO/LAO thin films with different thickness. From top to bottom: A: $t = 19$ nm, B: $t = 38$ nm, C: $t = 57$ nm, D: $t = 86$ nm, E: $t = 114$ nm. The diffraction peak of BFO (002) continuously shifts towards the small angle side with the increasing thickness, which is indicated by the vertical dashed line.

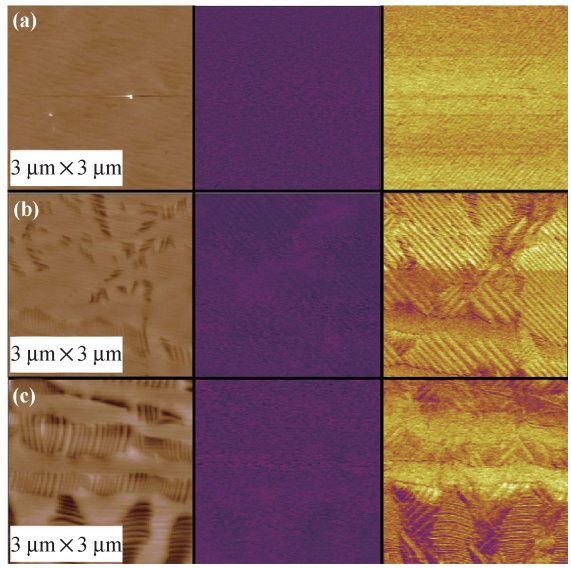

Fig. 2 Surface morphology (left, the height scale is 5 nm), out-of-plane phase (*middle*) and in-plane in-phase (*right*) piezoresponse force microscopy images for $t = 38$ nm **(a)**, 57 nm **(b)**, and 86 nm **(c)** samples. The PFM cantilever is oriented along the [100] direction during the PFM scanning.

IP-PFM images change significantly for samples with different thickness. For $t = 38$ nm, the surface is uniform and atomically smooth, suggesting a strained quasi-T phase. Slightly increasing t gives rise to some trenched regions, which is a signature of the coexisting quasi-T and R-phases as a result of strain relaxation [14]; the total area of these trenched regions increases with t. We also observed that the IP PFM images showed a clear stripe-like contrast within the quasi-T phase region, which suggests that some monoclinic distortion accompanies the quasi-T phase [21].

To get a better understanding of the thickness-dependent crystallographic distortion, we performed RSM of the (103)/(013) and (002) reflections. All the

spectra of (103)/(013) reflections [Figs. 3(a)–(d)] show the expected peak splitting, which can be associated to the multiple structural variants due to the epitaxial growth of the films [14]. This is consistent with the periodic IP stripe domains from the above PFM results, and the schematic drawing of the polarization for four downwards polarized domains are shown in Fig. 4(a). Here, one interesting feature worth mentioning is that an additional spot arises at $t = 57$ nm [Fig. 2(c)], and it becomes more pronounced at $t = 114$ nm [Fig. 3 (d)]. Similarly, for $t \geqslant 57$ nm, two symmetric satellite spots of the (002) reflections of the quasi-T phase can be seen as shown in Figs. 3(e) and (h). Such a phenomenon is not revealed previously [13, 14], and we attempt to interpret it by utilizing a twining structure model schematically shown in Fig. 4(b). For $t \leqslant 38$ nm, the films are fully strained, and all the variants are arranged in a normal configuration [illustrated in the bottom of Fig. 4(b)], so there is no additional spot in RSM. However, for $t \geqslant 57$ nm, a twining structure [illustrated in the top of Fig. 4(b)] takes form presumably due to the strain relaxation, which gives rise to the satellite spots of (002) reflections [Figs. 2(g) and (h)] as well as the fourth spot near the (103)/(013) reflections [Fig. 2(c) and (d)]. Based on this model, the twining angle should be the same as the monoclinic-like angle ($\beta - 90°$) of the quasi-T phase. Indeed, the twining angle ($\sim 1.89°$) is very close to the monoclinic-like angle ($\beta - 90° \sim 1.90(0.07)$). In addition, for the sample with the largest thickness of 114 nm, there exist several additional diffraction spots in the (002) mapping image as indicated by dot and solid circles in Fig. 2(h). For the spot indicated by dot circle, the corresponding c value is estimated to be ~ 3.98 Å, which matches well with the R-phase BFO [1, 5]. For the symmetric spots indicated by solid circles, the estimated c value is ~ 4.13 Å, which is also close to the value of R-phase BFO 1, 5]. However, a few recent reports have proposed that they should originate from another set of quasi-T phase BFO but with large tilting angles [17, 18]. Nevertheless, the complex crystalline structure of BFO/LAO thin films clearly warrants further investigations.

The thickness dependent lattice parameters of the quasi-T phase are obtained from the symmetric and asymmetric RSM data and shown in Figs. 4(c) and (d). The in-plane compression and the out-of-plane elongation agree with the previous reports [14]. Interestingly, we note that increasing the thickness causes a decrease in the tilting angle ($\beta - 90°$), but an increase in the OOP lattice c. This is essentially different from the case of R-phase BFO [24], in which the strain relaxation causes an opposite evolving way for ($\beta - 90°$) and c as compared with the quasi-T phase BFO. This phenomenon is possibly due to the different ground states of films with different misfit strain. In addition, the lattice parameters show the largest changes around $t = 57$ nm, accompanying the multi-phase coexistence. This suggests a critical thickness around 57 nm, where the quasi-T and the R-phases are proximate to each other in the energy landscape and their mutual conversion is sensitive to the internal/external stimuli. Actually, a sharp phase transition from the quasi-T to the R phase caused by the misfit strain was theoretically predicted [19, 20].

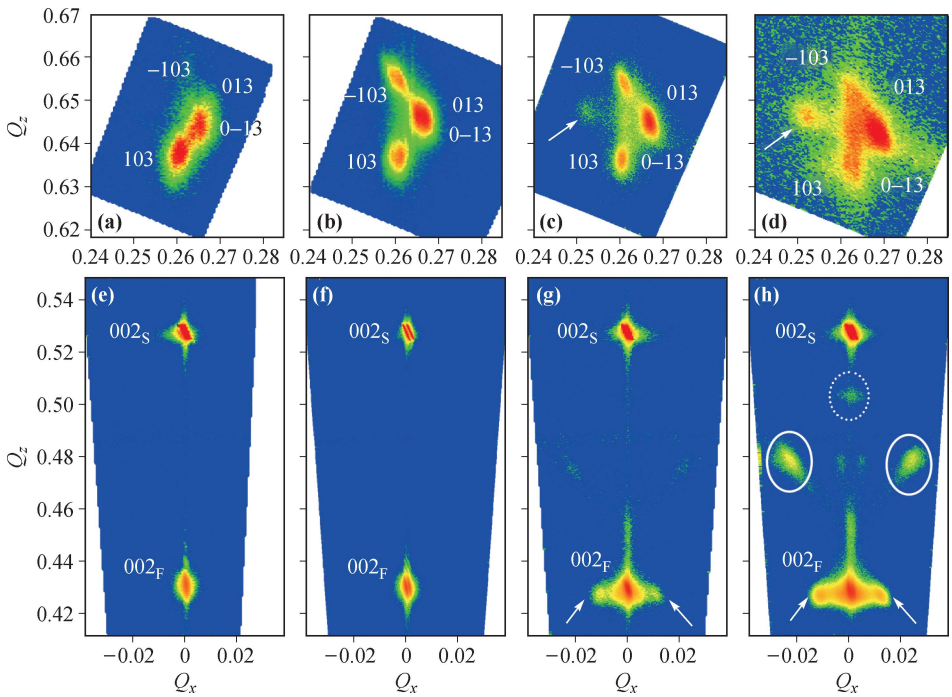

Fig. 3 Reciprocal space maps around (103)/(013) and (002) reflections of the quasi-tetragonal phase BFO in **(a)** and **(e)** 19 nm, **(b)** and **(f)** 38 nm, **(c)** and **(g)** 57 nm, **(d)** and **(h)** 114 nm films.

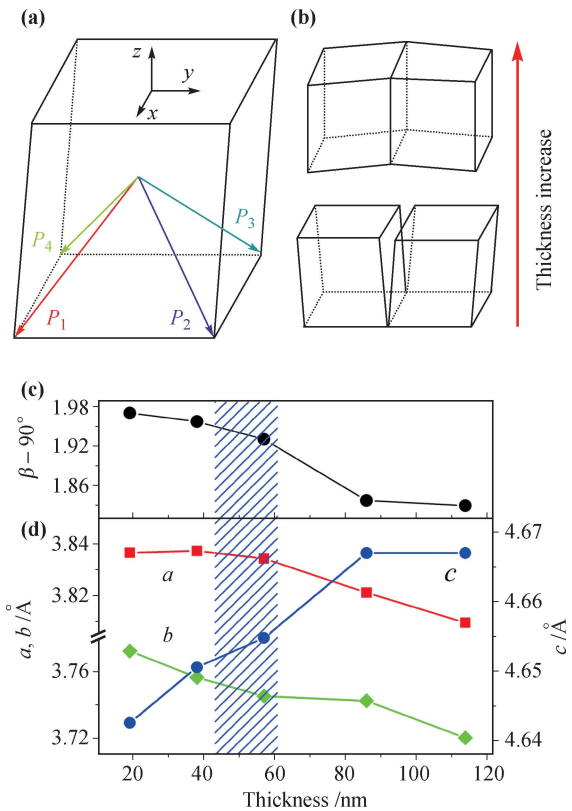

Fig. 4 Schematic drawing of **(a)** the polarization for four downward polarized domains, and **(b)** the evolution from normal state (bottom, such as the case in sample t = 38 nm) to twining structure (top, such as the case in sample t = 114 nm); **(c)** and **(d)** Thickness dependence of the cell parameters of the quasi-T phase BFO.

To study the instability of quasi-T phase BFO in the 38 nm sample that possesses the pure quasi-T phase, we took the topography and OOP/IP PFM images after a negative voltage (–10 V) writing. As presented in Fig. 5 (a), trenched regions appeared locally after the writing, which indicates the phase transition from the quasi-T to the R phase [13–19]. On the other hand, the PFM images of the written area did not show much change. Such a phase transition driven by the electric field can be phenomenologically understood using a schematic diagram of the energy landscape shown in Fig. 5(b). Although the R phase is favored as the ground state in the bulk BFO, the metastable quasi-T phase is preferred in the highly compressive strained BFO, and the small energy barrier between the two phases can be easily overcome by internal/external stimuli such as an electric field [12–19]. We noticed that very recently Mazumdar *et al.* [25] have reported on nanoscale switching between the quasi-T and R phases in BFO/LAO thin films with relatively large thickness $t > 70$ nm, in which the R-phase BFO already arises. Here, we focus on the structure instability of the quasi-T phase of BFO/LAO films with small thickness, which lies just near the phase boundary and no strain relaxation occurs. Different from Ref. [25], small electric field (10 V) was used to detect the delicate energy balance between the two phases in current work. Our results reveal that the quasi-T to R phase transition can only be observed in the sample t = 38 nm, which shows pure quasi-T phase and lies only within the blue shadow region (shown in Fig. 4). For the samples with larger or smaller thickness, no observable quasi-T and R phase change can be seen (not shown) when the writing voltage is 10 V or less, which suggests the absence of the phase transition and the larger energy barrier between the quasi-T and R phases within these samples. This is consistent with the theoretical prediction [11–14].

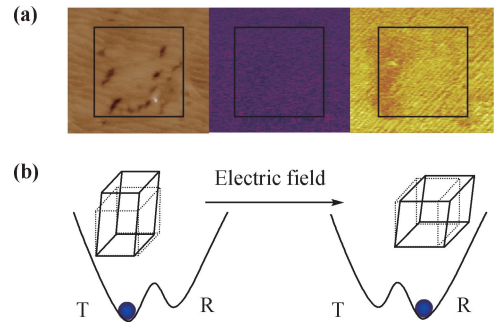

Fig. 5 Electric field driven phase transition in the sample with t = 38 nm. **(a)** Topography (left, height scale is 3 nm), out-of-plane (*middle*) and in-plane (*right*) piezoresponse force microscopy images, which was obtained after the film was poled with –10 V. The 1μm ×1 μm square demarcates the poled region. **(b)** Schematic energetic landscape showing the energy barrier between the quasi-tetragonal and the rhombohedral phases in the BFO thin film.

In conclusion, we synthesized and characterized high quality $BiFeO_3$ thin films with different thickness grown on (001) $LaAlO_3$ substrates with a large misfit strain of 4.8%. The highly strained quasi-tetragonal $BiFeO_3$ phase with a large $c \sim 4.66$ Å was obtained, and in-plane periodic nanodomains were observed along with the multi-phase coexistence. The reciprocal space mapping revealed interesting twining quasi-tetragonal phase BFO caused by the strain relaxation. In addition, an electric field driven phase transition was evidenced in the sample t = 38 nm, which showed small energy barrier between the meta-stable quasi-tetragonal phase and rhombohedral one.

Acknowledgements The authors acknowledge supports from the Singapore National Research Foundation, the National Natural Science Foundation of China (Grant Nos. 11104090 and 50832002), National Key Projects for Basic Research of China (Grant No. 2009CB929501), and the Priority Academic Program Development of Jiangsu Higher Education Institutions, China.

References

1. J. Wang, J. B. Neaton, H. Zheng, V. Nagarajan, S. B. Ogale, B. Liu, D. Viehland, V. Vaithyanathan, D. G. Schlom, U. V. Waghmare, N. A. Spaldin, K. M. Rabe, M. Wuttig, and R. Ramesh, Science, 2003, 299(5613): 1719
2. T. Zhao, A. Scholl, F. Zavaliche, K. Lee, M. Barry, A. Do-

ran, M. P. Cruz, Y. H. Chu, C. Ederer, N. A. Spaldin, R. R. Das, D. M. Kim, S. H. Baek, C. B. Eom, and R. Ramesh, Nat. Mater., 2006, 5(10): 823

3. K. F. Wang, J.-M. Liu, and Z. F. Ren, Adv. Phys., 2009, 58: 321
4. C. H. Yang, J. Seidel, S. Y. Kim, P. B. Rossen, P. Yu, M. Gajek, Y. H. Chu, L. W. Martin, M. B. Holcomb, Q. He, P. Maksymovych, N. Balke, S. V. Kalinin, A. P. Baddorf, S. R. Basu, M. L. Scullin, and R. Ramesh, Nat. Mater., 2009, 8(6): 485
5. G. Catalan and J. F. Scott, Adv. Mater., 2009, 21(24): 1
6. S. Y. Yang, J. Seidel, S. J. Byrnes, P. Shafer, C. H. Yang, M. D. Rossell, P. Yu, Y. H. Chu, J. F. Scott, L. W. Ager, L. W. Martin, and R. Ramesh, Nat. Nanotechnol., 2010, 5(2): 143
7. S. Fujino, M. Murakami, V. Anbusathaiah, S. H. Lim, V. Nagarajan, C. J. Fennie, M. Wuttig, L. Salamanca-Riba, and I. Takeuchi, Appl. Phys. Lett., 2008, 92(20): 202904
8. D. Kan, L. Palova, V. Anhusathaiah, C. J. Cheng, S. Fujino, V. Nagarajan, K. M. Rabe, and I. Takeuchi, Adv. Funct. Mater., 2010, 20(7): 1108
9. C. J. Cheng, D. Kan, S. H. Lim, W. R. Mckenzie, P. R. Munroe, L. G. Salamanca-Riba, R. L. Withers, I. Takeuchi, and V. Nagarajan, Phys. Rev. B, 2009, 80(1): 014109
10. F. Kubel and H. Schmid, Acta Crystallogr. B, 1990, 46(6): 698
11. N. A. Hill, J. Phys. Chem. B, 2000, 104(29): 6694
12. C. Ederer and N. A. Spaldin, Phys. Rev. Lett., 2005, 95(25): 257601
13. H. Béa, B. Dupé, S. Fusil, R. Mattana, E. Jacquet, B. Warot-Fonrose, F. Wilhelm, A. Rogalev, S. Petit, V. Cros, A. Anane, F. Petroff, K. Bouzehouane, G. Geneste, B. Dkhil, S. Lisenkov, I. Ponomareva, L. Bellaiche, M. Bibes, and A. Barthélémy, Phys. Rev. Lett., 2009, 102(21): 217603
14. R. J. Zeches, M. D. Rossell, J. X. Zhang, A. J. Hatt, Q. He, C. H. Yang, A. Kumar, C. H. Wang, A. Melville, C. Adamo, G. Sheng, Y. H. Chu, J. F. Ihlefeld, R. Erni, C. Ederer, V. Gopalan, L. Q. Chen, D. G. Schlom, N. A. Spaldin, L. W. Martin, and R. Ramesh, Science, 2009, 326(5955): 977
15. C. J. Cheng, C. L. Lu, Z. H. Chen, L. You, L. Chen, J. Wang, and T. Wu, Appl. Phys. Lett., 2011, 98(24): 242502
16. J. X. Zhang, Q. He, M. Trassin, W. Luo, D. Yi, M. D. Rossell, P. Yu, L. You, C. H. Wang, C. Y. Kuo, J. T. Heron, Z. Hu, R. J. Zeches, H. J. Lin, A. Tanaka, C. T. Chen, L. H. Tjeng, Y. H. Chu, and R. Ramesh, Phys. Rev. Lett., 2011, 107(14): 147602
17. A. R. Damodaran, C. W. Liang, Q. He, C. Y. Peng, L. Chang, Y. H. Chu, and L. W. Martin, Adv. Mater., 2011, 23(28): 3170
18. Z. H. Chen, S. Prosandeev, Z. L. Luo, W. Ren, Y. J. Qi, C. W. Huang, L. You, C. Gao, I. A. Kornev, T. Wu, J. Wang, P. Yang, T. Sritharan, L. Bellaiche, and L. Chen, Phys. Rev. B, 2011, 84(9): 094116
19. A. J. Hatt, N. A. Spaldin, and C. Ederer, Phys. Rev. B, 2010, 81(5): 054109
20. B. Dupé, I. C. Infante, G. Geneste, P. E. Janolin, M. Bibes, A. Barthélémy, S. Lisenkov, L. Bellaiche, S. Ravy, and B. Dkhil, Phys. Rev. B, 2010, 81(14): 144128
21. Z. H. Chen, Z. L. Luo, C. W. Huang, Y. J. Qi, P. Yang, L. You, C. S. Hu, T. Wu, J. L. Wang, C. Gao, T. Sritharan, and L. Chen, Adv. Funct. Mater., 2011, 21(1): 133
22. C. L. Lu, Y. Wang, L. You, X. Zhou, H. Y. Peng, G. Z. Xing, E. E. M. Chia, C. Panagopoulos, L. Chen, J. M. Liu, J. Wang, and T. Wu, Appl. Phys. Lett., 2010, 97(25): 252905
23. S. H. Xie, A. Gannepalli, Q. N. Chen, Y. M. Liu, Y. C. Zhou, R. Proksch, and J. Y. Li, Nanoscale, DOI: 10.1039/c1nr11099c
24. C. J. M. Daumont, S. Farokhipoor, A. Ferri, J. C. Wojdel, J. Íñiguez, B. J. Kooi, and B. Noheda, Phys. Rev. B, 2010, 81(14): 144115
25. D. Mazumdar, V. Shelke, M. Iliev, S. Jesse, A. Kumar, S. V. Kalinin, A. P. Baddorf, and A. Gupta, Nano Lett., 2010, 10(7): 2555